

Article

Numerical Analysis of Tube Heat Exchanger with Trimmed Star-Shaped Fins

Mladen Bošnjaković ^{1,*}  and Simon Muhič ² ¹ TECHDpt, University of Slavonski Brod, Trg Ivane Brlić Mažuranić 2, 35000 Slavonski Brod, Croatia² Institute for Renewable Energy and Efficient Exergy Use, Cesta 2. Grupe Odredov 17, 1295 Ivančna Gorica, Slovenia; simon.muhic@inoveks.si

* Correspondence: mbosnjakovic@unisb.hr

Abstract: In some engineering applications, it is very desirable that the heat exchanger is as light as possible while maintaining the heat transfer rate at an acceptable level. In this context, the possibility of reducing the weight of the heat exchanger with the star-shaped fins by cutting off the thermally least efficient part of the fin was investigated. For this purpose, the rear part of the fins was trimmed to Ø28, Ø31 and Ø34 mm. Numerical analysis was used to determine the influence of each variant on the flow characteristics in the air–water heat exchanger and on heat transfer for the range of $2300 < Re < 16,000$. The best results were obtained by trimming the rear part of the fin to Ø28 mm. With a 5.53% reduction in fin weight, heat transfer can be increased by up to 8.12% compared to the star-shaped fins without trimming. The pressure drop can be reduced by up to 0.92%. The trimmed fins were also compared with perforated star-shaped fins (perforation Ø2). At approximately the same weight, the trimmed fins increase the heat transfer coefficient by up to 5.75% with a reduction in pressure drop of up to 0.76% compared to the perforated fins.

Keywords: star-shaped fin; trimmed fins; heat exchanger; computational fluid dynamics



Citation: Bošnjaković, M.; Muhič, S. Numerical Analysis of Tube Heat Exchanger with Trimmed Star-Shaped Fins. *Appl. Sci.* **2022**, *12*, 4857. <https://doi.org/10.3390/app12104857>

Academic Editors: Huizhu Yang, Binjian Ma and Yu Feng

Received: 27 April 2022

Accepted: 9 May 2022

Published: 11 May 2022

Publisher's Note: MDPI stays neutral with regard to jurisdictional claims in published maps and institutional affiliations.



Copyright: © 2022 by the authors. Licensee MDPI, Basel, Switzerland. This article is an open access article distributed under the terms and conditions of the Creative Commons Attribution (CC BY) license (<https://creativecommons.org/licenses/by/4.0/>).

1. Introduction

Finned surfaces are often used for efficient heat exchange between liquids and gases. They are placed on the gas-side to increase the heat exchange area. In heat exchanger design, a common requirement is to have as little weight as possible, i.e., as little heat transfer area as possible. To meet this requirement, various geometric shapes of fins have been studied, based on analytical models of heat transfer on the extended surfaces and on numerical analysis and experimental studies.

Marcinkowski and Taler [1] presented a method for calculating the efficiency of fins of arbitrary shape mounted on tubes of arbitrary shape using the finite element method. The paper also analyses the accuracy of calculating the efficiency of fins with complex shape using analytical and approximated methods: equivalent circular fin methods and sector methods. Djefal et al. [2] examined eight configurations of finned oval and flat tubes and compared them with conventional circular tubes. The configuration was tested in the interval $2600 < Re < 10,200$. The analysis of the effects of the flatness of the tubes and the axial ratio of the oval tubes on the heat flow properties showed that tubes with higher flatness gave a better result. Nemati et al. [3] attempted to optimize the shape of the ring fins in a heat exchanger with multiple rows to improve thermal performance. They performed a numerical analysis and concluded that a local approach to optimize the fin shape is a good technique to further improve the performance of finned tube heat exchangers while reducing their cost.

Sundar et al. [4] numerically and experimentally tested serrated fins of 1 mm thickness with circular perforations under natural convection and radiation. They varied the fin width (4 to 7 mm), the number of perforations (0 to 3), and the size of the perforation (Ø2

to $\text{Ø}4$ mm). The results showed that the variant with perforated surfaces had about 7% to 12% lower thermal resistance than the nonperforated surfaces.

Tahrour et al. [5] analyzed the position of the tube in an annular fin that maximizes heat transfer and minimizes pressure drop. They used computational fluid dynamics (CFD) and the analysis was performed for the range $4500 \leq Re \leq 22,500$. For small fin spacing, an eccentrically placed tube in the fin is more efficient than a concentric one.

Petrik et al. [6] analyzed the cooling efficiency of a heat exchanger for cars using numerical analysis. The aim was to find the optimal shape of the heat exchanger that would reduce the coolant temperature to the required value and have the lowest weight.

Tahrour and Ahmad [7] studied the characteristics of five fin designs in tubular heat exchangers: a concentric annular fin, an eccentric annular fin, a perforated annular fin, a serrated fin and a star-shaped fin. The Reynolds number ranged from 4300 to 15,000, and the conventional concentric circular fins gave the lowest performance criterion, while the serrated fins gave the highest performance evaluation criterion. According to the criterion of weight performance, star-shaped fins achieved the best result.

Numerous researchers [8–16] have published papers in which they studied the effect of fin perforation on the flow characteristics in a heat exchanger. In general, all researchers concluded that perforation increases the degree of turbulence and thus improves heat transfer.

One of the proposals to reduce the weight of heat exchangers while improving heat transfer is to use star-shaped fins [17–20]. The authors designed a tubular heat exchanger with star-shaped fins and analyzed it using CFD simulation. The results were compared with the equivalent case of solid annular fins. With a 43.4% lower weight of the star-shaped fins compared to standard annular fins, the heat transfer coefficient of the star-shaped fins was 10% to 15% higher in the range $2300 < Re < 11,500$.

Recently, many other researchers have used CFD to study heat transfer properties [21–24].

2. Materials and Methods

The object of research is star-shaped fins mounted on tubes through which hot water flows. Cold air flows around the tubes and fins. In this work, the possibility of further reducing the weight of this type of heat exchanger and improving heat transfer by cutting off the least efficient part of the fin was investigated. A numerical analysis using computational fluid dynamics software was performed to analyze the flow characteristics in a modeled heat exchanger.

2.1. Geometric Description

The geometry of the heat exchanger is defined in [17–20]. Stainless steel was chosen as the material for the tubes and fins. Star-shaped fins with an outer diameter of 40 mm, a thickness of 0.5 mm and a height of 10 mm were attached to the $\text{Ø}20$ tube as reference geometry. The star arm on the back-side of the fin (as seen in the flow direction) is trimmed to a specific radius. Three trim radii were selected for analysis: $\text{Ø}28$, $\text{Ø}31$ and $\text{Ø}34$ mm. Figure 1 shows the case with $\text{Ø}28$ mm trim radius.

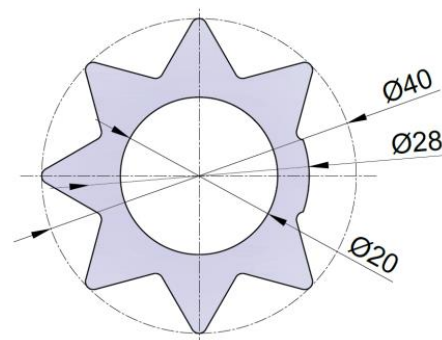


Figure 1. The trimmed star-shaped fin.

2.2. Numerical Analysis

The numerical analysis was performed analogously to that described in [17,18]. The same basic settings and boundary conditions were used. The computational domain is shown in Figure 2.

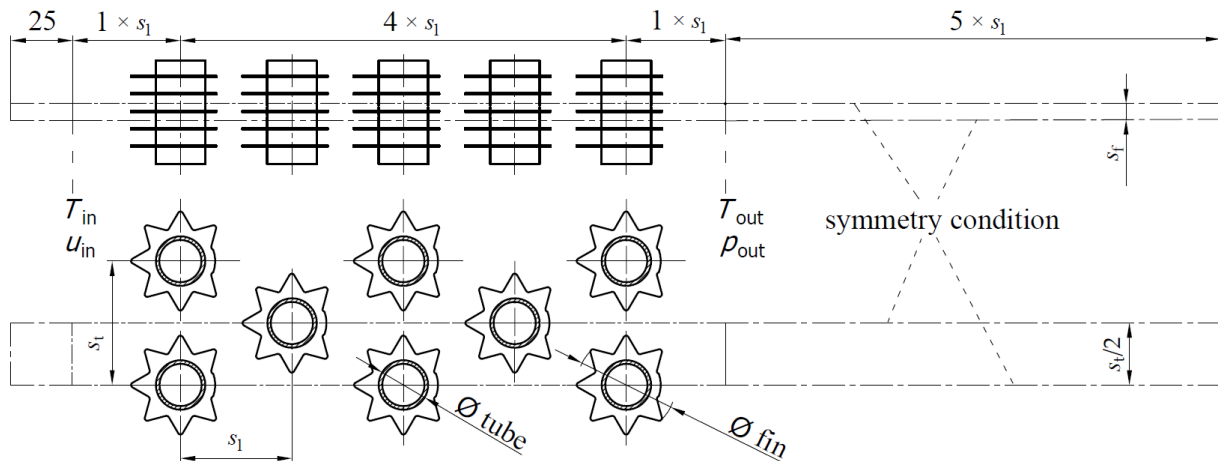


Figure 2. Computational domain.

In the mathematical description of the thermal phenomena in the heat exchangers, certain assumptions and simplifications were made. The usual assumptions used in defining fluid flow are continuity, homogeneity and isotropy of the fluid. The heat exchanger analyzed is of such a size that the conditions of the continuity hypothesis can be considered satisfied. The working medium, air, is considered as a single-component fluid that has the same physical properties at all points. Thus, the homogeneity condition is satisfied. The assumption of equal thermal conductivity of the fins in all directions (isotropy) was also adopted. The next assumption is that no medium escapes through the walls of the heat exchanger and that no heat is released to the environment. It is also assumed that there is no contact resistance between the tube and the surface at the base of the fin. A steady state analysis was performed.

The following assumptions were made for the boundary and initial conditions:

- The air entering the heat exchanger had a uniform velocity across the cross section. The turbulence intensity at inlet was set at 5%.
- The temperature of the air entering the heat exchanger was 288 K.
- Since water has a high heat capacity, the temperature of the inner wall of the tube was assumed to be constant and equal to the water temperature.
- The symmetry condition was set on the sides of the calculation area.
- Additionally, the symmetry condition was set for the left, right, bottom and top sides of the calculation area.
- The normal velocity component on the symmetry plane was zero; i.e., there was no convective flow through the symmetry plane. Therefore, the temperature gradients and the tangential components of the velocity gradients in the normal direction were set to zero.

Tables 1 and 2 contain the dimensional data and the boundary conditions for the heat transfer analysis.

Table 1. Data of the tube and the star-shaped fin.

Item	Variable	Unit	Value
Material	-	-	stainless steel
Tube data	d_0	mm	20
	-	-	staggered
	s_t	mm	50
	s_l	mm	40
	N_l	-	5
Fin data	t_f	mm	0.5
	s_f	mm	4.5
Trimming diameter	-	mm	28, 31 and 34

Table 2. Boundary conditions.

Boundary Condition	Variable	Unit	Value
Temperature of air at the inlet	T_{in}	K	288
Air velocity at the inlet	u_{in}	m/s	1, 2, 3, 5 and 7
Temperature of the tube internal wall	T_w	K	353
Gauge air pressure at the outlet of the heat exchanger	p_{out}	Pa	0
Condition at the air-side tube wall			Hydraulically smooth wall

2.3. Governing Equations

The applied mathematical model consists of a set of differential equations and constitutive relations, together with boundary and initial conditions. Conservation law of mass:

$$\frac{\partial \rho}{\partial t} + \frac{\partial(\rho u_j)}{\partial x_j} = 0 \quad (1)$$

Conservation law of momentum:

$$\frac{\partial(\rho u_j)}{\partial t} + \frac{\partial(\rho u_j u_i)}{\partial x_j} = \rho f_i + \frac{\partial \sigma_{ji}}{\partial x_j} \quad (2)$$

Conservation law of energy:

$$\frac{\partial(\rho e)}{\partial t} + \frac{\partial(\rho e u_j)}{\partial x_j} = -\rho f_i u_i + \frac{\partial(\sigma_{ji} u_i)}{\partial x_j} - \frac{\partial q_j}{\partial x_j} \quad (3)$$

The finite volume method is commonly used to solve a defined mathematical model. The computational domain was meshed using ANSYS Meshing software, version 17.2. A hybrid mesh approach was used. This means that the larger part of the volume is meshed with a structured mesh, while the remaining volume is meshed with an unstructured mesh. Eight inflation layers were defined in the area of convective heat transfer from tubes and fins to the air. Figure 3 shows a 3D view of the reference geometry (a) and detail of the mesh (b).

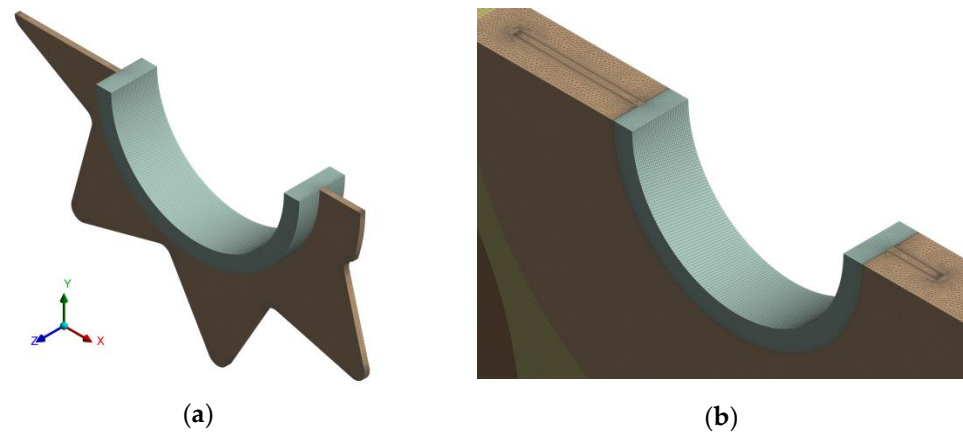


Figure 3. Three-dimensional view of the trimmed fin (a) and the mesh detail (b).

Mesh independence analysis was performed, focused mainly on Nu and Eu . The results are shown in Figures 4 and 5.

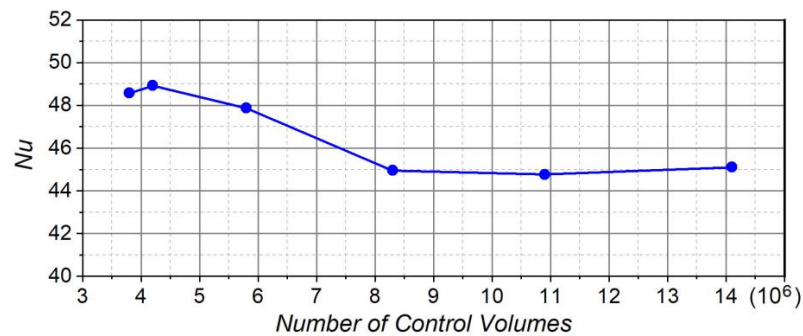


Figure 4. Nu at mesh independence analysis.

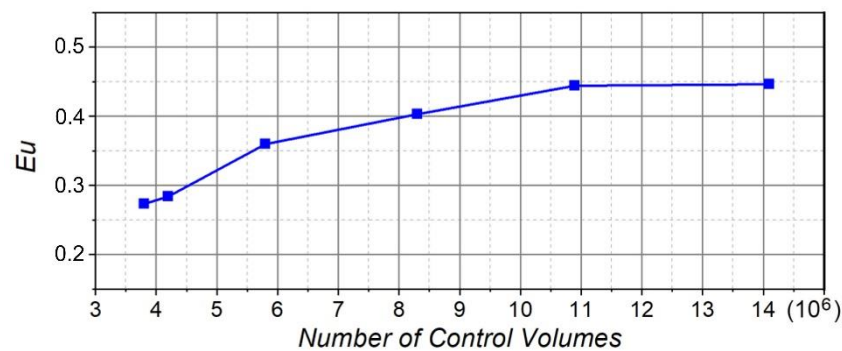


Figure 5. Eu at mesh independence analysis.

For this analysis, we chose a 14.5 million volume mesh and the $k-\omega$ SST turbulence model described in detail in [17].

3. Results and Discussion

An important aspect of numerical simulations is to assess whether or not the simulation is complete and convergent. The most commonly used method to check this is to examine the residuals for each variable to be solved. The default convergence criterion in ANSYS Fluent states that the residuals for all equations solved must be reduced to 10^{-3} , except for the energy equation, for which the criterion is set at 10^{-6} . In our case, more stringent criteria of 10^{-4} and 10^{-9} , respectively, were chosen. The convergence error is compared with the amount of heat released from the inner wall of the tube through the

outer surface of the tube and the fins, and with the amount of heat absorbed by the air. The maximum deviation is about 0.08%.

The results of the CFD simulations are shown in Tables 3–6.

Table 3. Output data for the trimming diameter of 28 mm.

Velocity of Air at Inlet u_{in} (m/s)	Temperature of Air at Outlet T_{out} (K)	Pressure Drop in the Tube Bundle Δp (Pa)	Mean Fins Surface Temperature (K)	Mean Temperature of the Tubes Outer Surface (K)
1.0	322.25	10.24	342.20	352.44
2.0	313.09	35.49	338.22	352.19
3.0	308.75	75.31	335.62	352.00
5.0	304.27	195.80	331.87	351.70
7.0	301.88	368.51	329.07	351.46

Table 4. Output data for the trimming diameter of 31 mm.

Velocity of Air at Inlet u_{in} (m/s)	Temperature of Air at Outlet T_{out} (K)	Pressure Drop in the Tube Bundle Δp (Pa)	Mean Fins Surface Temperature (K)	Mean Temperature of the Tubes Outer Surface (K)
1.0	322.25	10.24	342.37	352.44
2.0	313.30	35.61	338.39	352.18
3.0	308.79	75.26	335.79	352.00
5.0	304.31	195.72	332.03	351.70
7.0	301.91	368.33	329.21	351.46

Table 5. Output data for the trimming diameter of 34 mm.

Velocity of Air at Inlet u_{in} (m/s)	Temperature of Air at Outlet T_{out} (K)	Pressure Drop in the Tube Bundle Δp (Pa)	Mean Fins Surface Temperature (K)	Mean Temperature of the Tubes Outer Surface (K)
1.0	322.18	10.24	342.48	352.44
2.0	313.30	35.60	338.47	352.18
3.0	308.82	75.29	335.86	352.00
5.0	304.33	195.86	332.07	351.70
7.0	301.94	368.95	329.21	351.45

Table 6. Output data for the star-shaped fins without trimming.

Velocity of Air at Inlet u_{in} (m/s)	Temperature of Air at Outlet T_{out} (K)	Pressure Drop in the Tube Bundle Δp (Pa)	Mean Fins Surface Temperature (K)	Mean Temperature of the Tubes Outer Surface (K)
1.0	321.97	10.27	342.59	352.45
2.0	313.28	35.82	338.52	352.19
3.0	308.92	75.86	335.85	352.00
5.0	304.40	197.11	332.02	351.70
7.0	301.98	371.33	329.13	351.45

The results of CFD simulations for star-shaped fins with perforation are presented in [12].

3.1. Data Reduction and Interpretation

The calculation of the dimensionless numbers Nu , Pr and Eu is based on the physical properties of the working fluid, which depend on the temperature and pressure. For an accurate calculation of the dimensionless characteristics, it is necessary to determine the exact temperature at which the physical properties of the working medium are measured. This temperature is the boundary layer temperature, which is defined as follows:

$$T_{bl} = (T_w + T_{av})/2 \quad (4)$$

The average temperature of the free air flow is considered at

$$T_{av} = (T_{in} + T_{out})/2 \quad (5)$$

For the calculation of the Re number, the density and the dynamic viscosity are applied to the average air temperature T_{av} . The outer diameter of the tube is taken as the characteristic dimension (L). The characteristic air velocity (u_{ff}) is the air velocity through the narrowest flow section within the tube bundle.

$$Re = \frac{\rho_{av} \cdot u_{ff} \cdot L}{\mu_{av}} \quad (6)$$

The narrowest area of free flow is between the tubes in the transverse direction and can be expressed as follows:

$$A_{ff} = s_f \cdot (s_l - d_0) - 2 \cdot h_f \cdot t_f \quad (7)$$

The dimensionless Nusselt number is defined as follows:

$$Nu = \frac{\alpha_0 \cdot d_0}{\lambda_{bl}} \quad (8)$$

where α_0 is the actual average heat transfer coefficient on the air-side. The expression for the dimensionless Eu number is:

$$Eu = \frac{\Delta p}{N_1 \cdot \rho_{av} \cdot u_{ff}^2} \quad (9)$$

Thermal performance is calculated based on mass air flow and total temperature change.

$$\dot{m} = \rho_{in} \cdot A_{tot} \cdot u_{in} \quad (10)$$

$$Q_{air} = \dot{m} \cdot c_{p,av} \cdot (T_{out} - T_{iu}) \quad (11)$$

The total heat transfer coefficient (U) is calculated using the log average method (LMTD).

$$\Delta T_{ln} = \frac{T_{in} - T_{out}}{\ln \frac{T_{in} - T_w}{T_{out} - T_w}} \quad (12)$$

T_w is the temperature of the inner wall of the tube, i.e., the water in the tube. The total heat transfer coefficient can be calculated as follows:

$$U = \frac{Q_{air}}{A \cdot \Delta T_{ln}} \quad (13)$$

The heat transfer coefficient on air-side can be calculated as follows:

$$\alpha_e = \frac{1}{\left(\frac{1}{U} - A_{tot} \frac{\ln \frac{d_0}{d_i}}{2\pi L_t \lambda} - \frac{A_{tot}}{A_i \alpha_i} \right)} \quad (14)$$

The effective heat transfer coefficient in Equation (14) is the apparent heat transfer coefficient and includes the fin efficiency. To calculate the actual average heat transfer coefficient (α_0), the efficiency of the fin η_f must first be calculated.

It was assumed that the heat transfer coefficient on the tube-side is large enough (several thousand $W/(m^2K)$) so that the last term in the denominator is approximately zero.

$$\alpha_0 = \frac{\alpha_e \cdot A_{tot}}{(A_t + \eta_f \cdot A_f)} \quad (15)$$

Fin efficiency is calculated using the average fin surface temperature from the numerical analysis (see Tables 3–6).

$$\eta_f = 1 - \frac{(T_W - T_{f,av}) \cdot \alpha_e}{U \cdot (T_W - T_{av})} \quad (16)$$

The pressure drop in the tube bundle is calculated using the following formula:

$$\Delta p = p_{in} - p_{out} \quad (17)$$

where p_{in} and p_{out} are the mass-weighted average pressures at the inlet and outlet of the tube bundle, respectively, obtained from the numerical analysis.

3.2. Flow Characteristics

Flow characteristics were analyzed for a tube bundle with five staggered rows of tubes. The material of the tubes and fins is stainless steel with a thermal conductivity of $16 W/(m^2K)$. All figures below show the flow characteristics for the star-shaped fins and the trimmed star-shaped fins at a diameter of 28 mm. Cases for other trimming diameters are not shown because they were similar to the case shown.

The global temperature, velocity, kinetic turbulence energy and pressure distribution in the heat exchanger bundle are important for the comprehension of the local flow and heat transfer processes. The thermal conductivity of the fin material strongly affects the temperature distribution along the fin. In our case, the fin is thin and the temperature differences in the transverse direction within the fin are small compared to the temperature differences between the fin and the environment.

Figure 6 presents the local feature of the temperature fields for analyzed fins. The temperature field over the fin area is not uniform and the temperature of the fin tip is different for each needle. The temperature profile for both variants is almost the same. The average temperature of the trimmed fins is lower by less than 1 K.

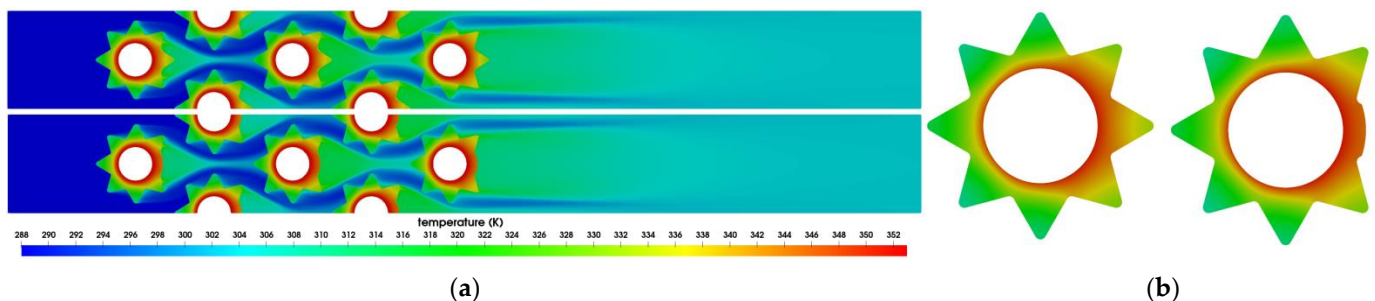


Figure 6. Temperature fields (a) for star-shaped fins and trimmed fins; (b) fin temperatures in the third row (middle section).

The velocity fields, turbulence kinetic energy fields, pressure-drop fields, and y^+ fields for star-shaped fins and trimmed fins are almost identical (Figures 7–10).

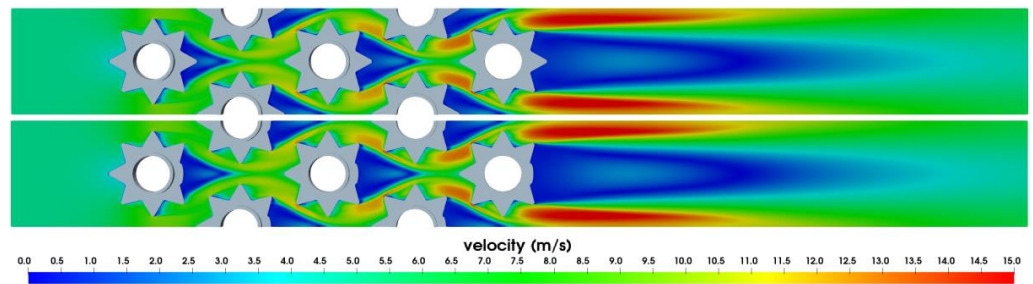


Figure 7. Velocity fields for star-shaped fins and trimmed fins.

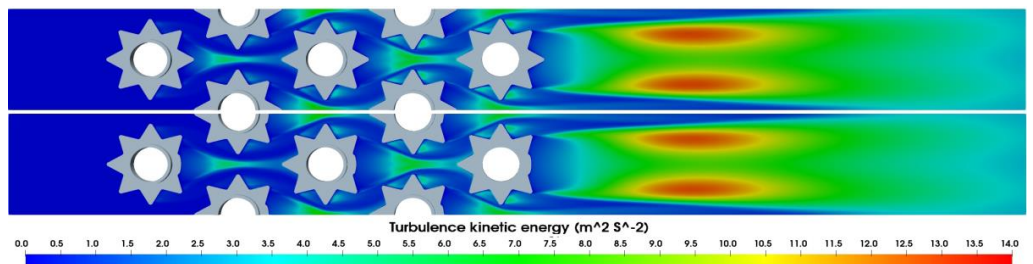


Figure 8. Turbulent kinetic energy fields for star-shaped fins and trimmed fins.

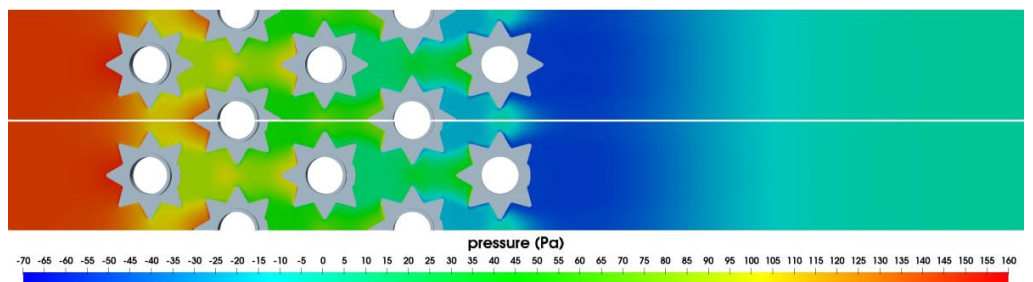


Figure 9. Pressure-drop fields for star-shaped fins and trimmed fins.

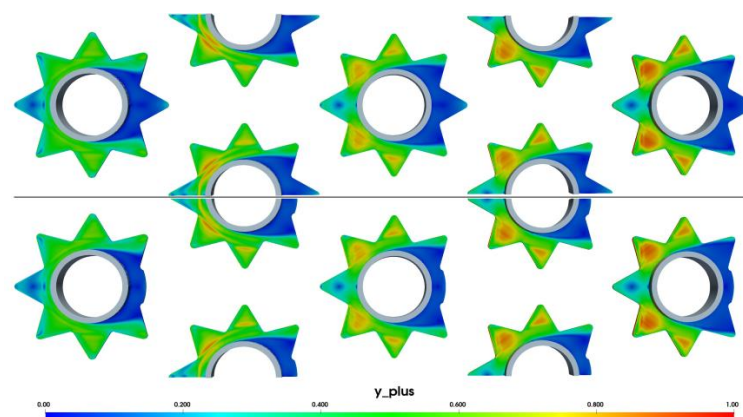


Figure 10. The y^+ fields for star-shaped fins and trimmed fins.

The fluid particles on the middle plane hit the tube at the stagnation point, bringing the fluid to a standstill and thus increasing the pressure at that point. The pressure decreases in the direction of flow while the velocity of the liquid increases.

A wake region is formed behind the tubes, and vortex formation is particularly evident after the fifth row of the tube. In this region, the pressure is much lower than the pressure at the stagnation point. Owing to the lower air velocity in the wake regions, heat exchange is lower and temperatures are higher.

The degree of turbulence and thus the difference in heat transfer coefficient increases with the number of rows due to the combined effects of the upstream rows.

Figure 11 shows the dependence of the Nu number on the Re number for the star-shaped fins, the perforated star-shaped fins (see [12]) and for the fins cut to diameters of 28, 31 and 34 mm. From the figure, it can be seen that the worst results are obtained with the ordinary star-shaped fins, while the best results are obtained with the perforated fins and the fins with a cut diameter of 28 mm.

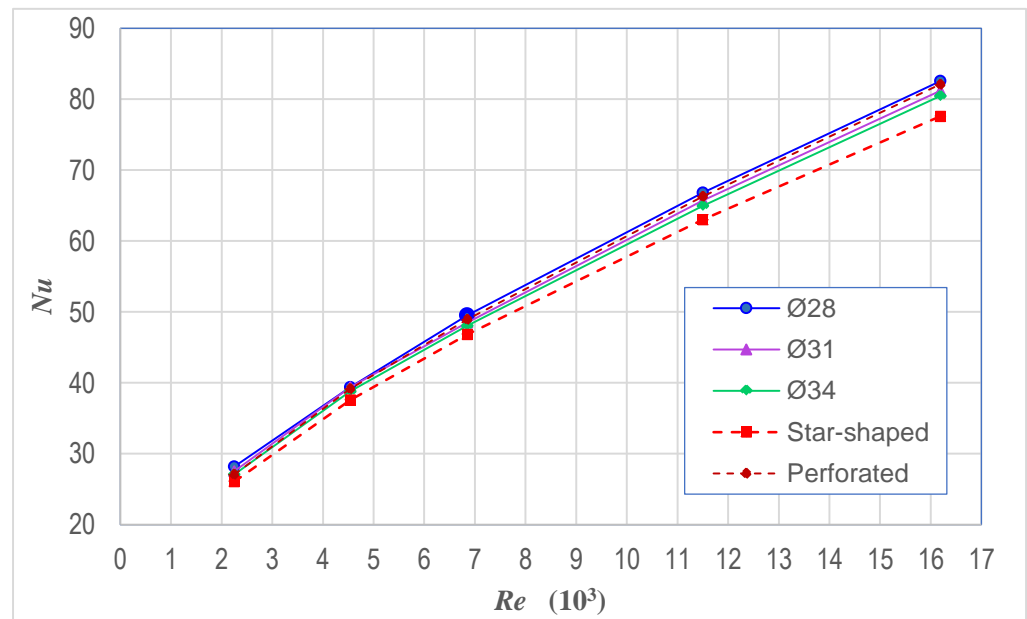


Figure 11. Nu number versus Re .

Figure 12 shows the efficiency of the fins. From the figure, it can be seen that in the range of small Re numbers there is a small difference in efficiency between the studied fins. At higher Re numbers, the perforated fins are the least efficient, and the ordinary star-shaped fins have the highest efficiency. The efficiency of the trimmed fins is very similar to the efficiency of the ordinary star-shaped fins.

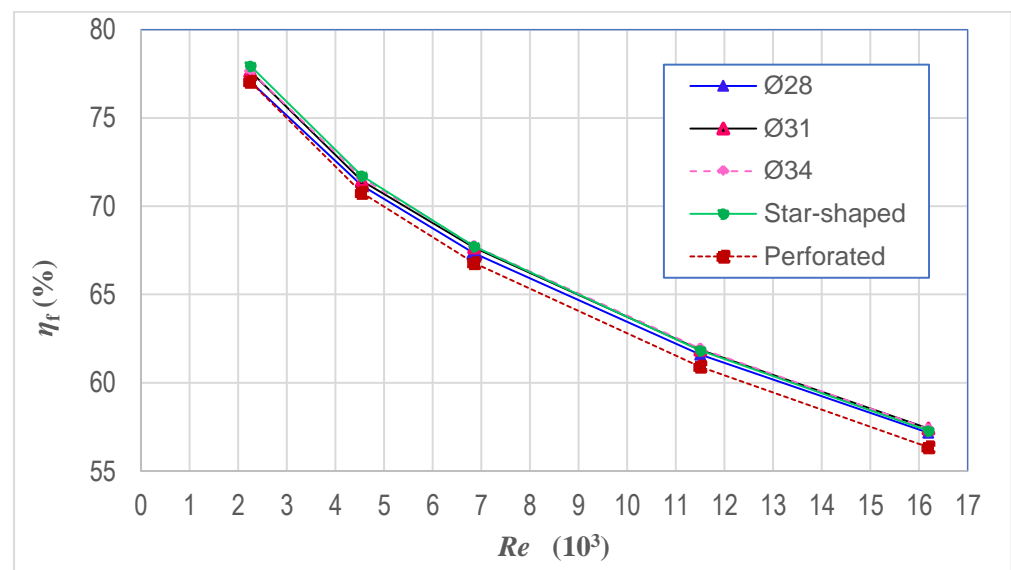


Figure 12. Fin efficiency.

Figure 13 shows the dependence of the heat transfer coefficient on the Re number. The results are similar to those in Figure 11. It can be seen from Figure 13 that the worst results are obtained by the ordinary star-shaped fins, while the best results come from the perforated fins and the fins with a trim diameter of 28 mm.

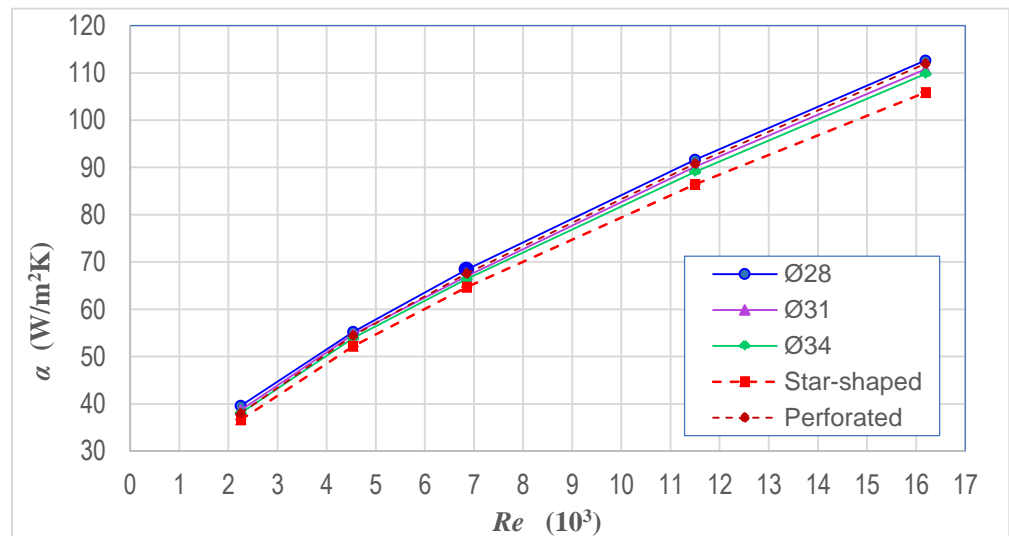


Figure 13. Heat transfer coefficient versus Re number.

Figure 14 shows the dependence of the heat transfer coefficient on the efficiency of the fins. From this figure, it can be seen that the best heat transfer results are obtained with trimmed fins. The fin trimmed to a diameter of 28 mm achieves the best result because the part that has the lowest heat transfer efficiency has been removed. This difference is particularly noticeable in the lower fin efficiencies obtained at higher airflow velocities through the heat exchanger. The heat transfer coefficient can be increased by up to 8.12% compared to the star-shaped fins without trim and by up to 5.75% compared to the perforated star-shaped fins.

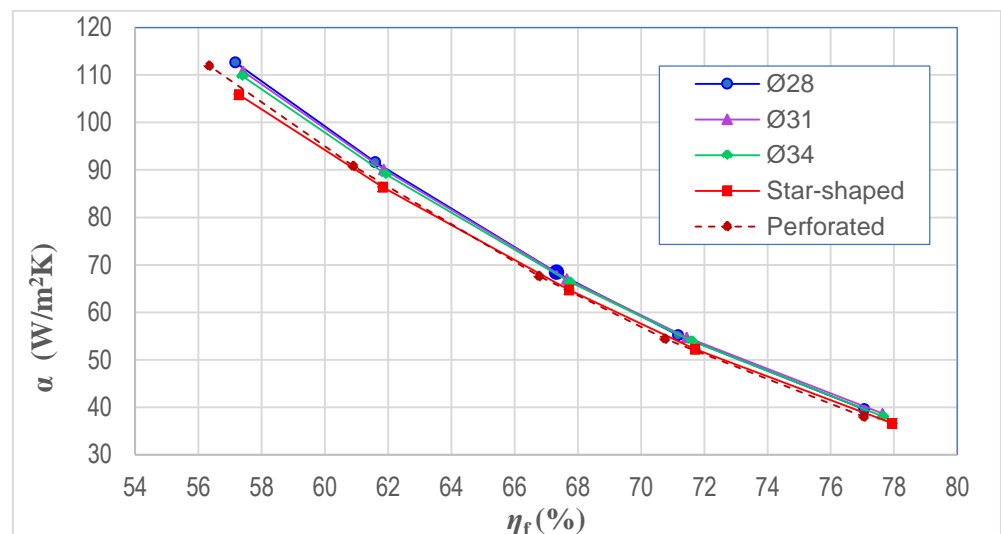


Figure 14. Heat transfer coefficient versus fin efficiency.

Figure 15 shows the dependence of the heat flux on the Re number. From this figure, it can be seen that the best heat transfer results are obtained with trimmed fins, and specifically with fins trimmed to a diameter of 28 mm. Ordinary star-shaped fins have the worst result. This is consistent with the results shown in Figures 11 and 13.

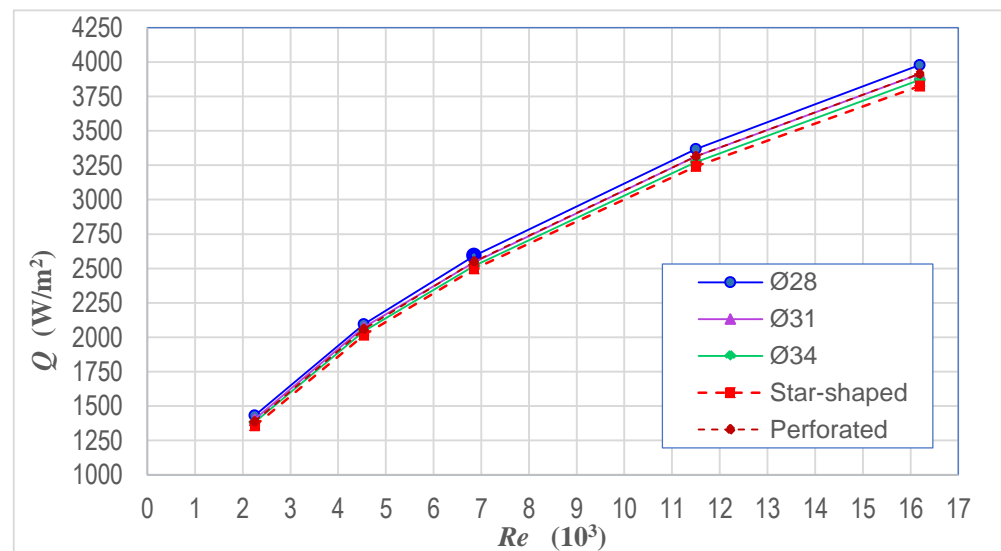


Figure 15. Heat flux versus Re number.

The influence of the studied variants on the pressure drop is shown in Figure 16. From the figure, it can be seen that there is no significant influence on the amount of Eu number. Trimmed fins lead to slightly better results in the range of higher Re numbers. The reduction in pressure drop is up to 0.76% compared to the perforated fins and up to 0.92% compared to the ordinary star-shaped fins in the observed range of Re numbers.

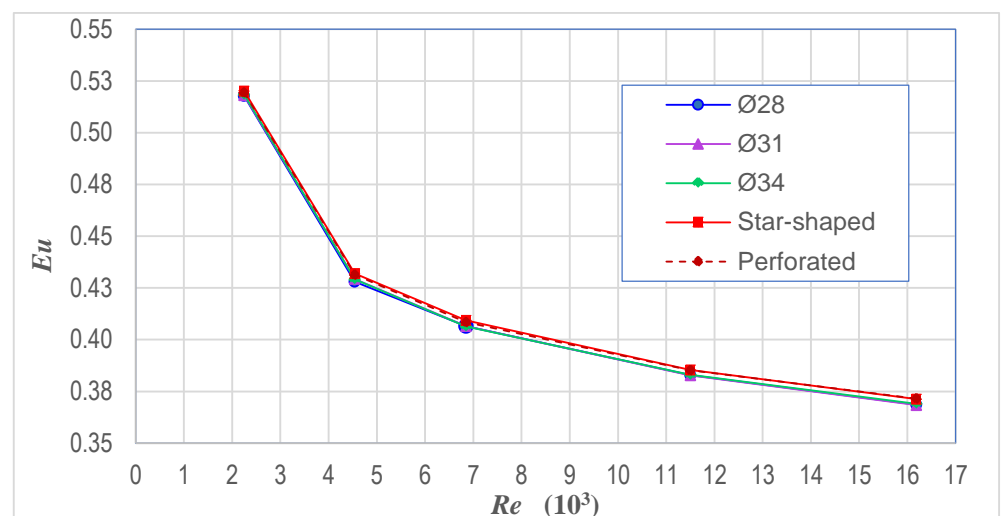


Figure 16. Euler number versus Re number.

4. Conclusions

In this study, another way to increase the heat exchange performance while reducing the weight of the heat exchanger for the star-shaped fins was investigated. The previously studied star-shaped fin with a diameter of 40 mm was selected as a reference case for weight reduction. This innovative idea consists in reducing the weight by trimming the star arm on the back-side of the fin. Three trim radii were analyzed in the study, Ø34, Ø31 and Ø28 mm. Using this approach, we were able to reduce the weight of the fin by 1.6%, 3.3% and 5.5%, respectively. From the study it can be concluded that trimming the rear part of the fin, which is the least efficient in heat exchange, can increase the average heat transfer coefficient by up to 8.12% compared to the star-shaped fins without trimming and by up to 5.75% compared to the perforated star-shaped fins. This is achieved with a weight reduction of 5.5% compared to the heat exchanger with the star-shaped fins without

trimming. The fin trimmed to a diameter of 28 mm performed better compared to other analyzed cases with larger trim radius or compared to previously analyzed cases with perforated fins.

Author Contributions: M.B.: conceptualization, methodology, writing—original draft preparation, visualization, data curation; S.M.: software, visualization, supervision and editing. All authors have read and agreed to the published version of the manuscript.

Funding: This research received no external funding.

Institutional Review Board Statement: Not applicable.

Informed Consent Statement: Not applicable.

Data Availability Statement: The data presented in this study are available on request from the corresponding author.

Conflicts of Interest: The authors declare no conflict of interest.

Nomenclature

A_f	surface area	m^2
A_i	tube inside surface area	m^2
A_{tot}	total heat transfer area on air-side	m^2
d_o	outside tube diameter	mm
$c_{p,av}$	air specific heat capacity for T_{av}	J/(kg·K)
Eu	Euler number	-
f	friction factor	-
f_i	vector of the mass density of the external forces	N/kg
h_f	fin height	mm
j	Colburn factor	-
\dot{m}	air mass flow	kg/s
N_1	number of tube rows in the flow direction	-
Nu	Nusselt number	-
Δp	pressure drop	Pa
p_{out}	mass-weighted average pressure outlet of the channel	Pa
Q	heat flow rate	W
q	heat flux vector	W
Re	Reynolds number	-
s_f	fin pitch	mm
s_l	longitudinal tube pitch	mm
s_t	transverse tube pitch	mm
t	time	s
t_f	fin thickness	mm
T_{in}	air inlet temperature	K
T_{out}	air outlet temperature	K
T_w	tube wall temperature	K
T_{av}	mean air temperature in tube bundle	K
U	overall heat transfer coefficient	W/(m ² ·K)
u	air velocity	m/s
u_{ff}	air velocity at minimum flow area	m/s
u_{in}	air velocity at the inlet of the heat exchanger	m/s
α_0	actual average gas-side heat transfer coefficient	W/(m ² ·K)
α_e	effective heat transfer coefficient based on total fin-side surface area	W/(m ² ·K)
α_i	tube-side heat transfer coefficient	W/(m ² ·K)
$\eta_{f,th}$	theoretical fin efficiency	-
μ_{av}	average air kinematic viscosity	m ² /s
ρ_{av}	average air density (at mean air temperature in tube bundle)	kg/m ³
λ_{bl}	thermal conductivity of boundary layer	W/(m·K)

References

1. Marcinkowski, M.; Taler, D. Calculating the Efficiency of Complex-Shaped Fins. *Energies* **2021**, *14*, 577. [[CrossRef](#)]
2. Djeflal, F.; Bordja, L.; Rebhi, R.; Inc, M.; Ahmad, H.; Tahrouf, F.; Ameer, H.; Menni, Y.; Lorenzini, G.; Elagan, S.K.; et al. Numerical Investigation of Thermal-Flow Characteristics in Heat Exchanger with Various Tube Shapes. *Appl. Sci.* **2021**, *11*, 9477. [[CrossRef](#)]
3. Nemati, H.; Moghimi, M.A.; Sapin, P.; Markides, C.N. Shape optimisation of air-cooled finned-tube heat exchangers. *Int. J. Therm. Sci.* **2020**, *150*, 106233. [[CrossRef](#)]
4. Sundar, S.; Song, G.; Zahir, M.Z.; Jayakumar, J.S.; Yook, S.-J. Performance investigation of radial heat sink with circular base and perforated staggered fins. *Int. J. Heat Mass Transf.* **2019**, *143*, 118526. [[CrossRef](#)]
5. Tahrouf, F.; Benmachiche, A.H.; Aksas, M.; Bougriou, C. 3-d numerical study and comparison of eccentric and concentric annular-finned tube heat exchangers. *J. Eng. Sci. Technol.* **2015**, *10*, 1508–1524.
6. Petrik, M.; Szepesi, G.; Jármai, K. CFD analysis and heat transfer characteristics of finned tube heat exchangers. *J. Inf. Sci. Eng.* **2019**, *14*, 165–176. [[CrossRef](#)]
7. Tahrouf, F.; Ahmad, H.; Ameer, H.; Saeed, T.; Abu-Zinadah, H.; Menni, Y. 3D numerical study and comparison of thermal-flow performance of various annular finned-tube designs. *J. Ocean Eng. Sci.* **2022**. [[CrossRef](#)]
8. Ibrahim, T.K.; Al-Sammarraie, A.T.; Al-Jethelah, M.S.M.; Al-Doori, W.H.; Salimpour, M.R.; Tao, H. The impact of square shape perforations on the enhanced heat transfer from fins: Experimental and numerical study. *Int. J. Therm. Sci.* **2020**, *149*, 106144. [[CrossRef](#)]
9. Nadooshan, A.A.; Kalbasi, R.; Afrand, M. Perforated fins effect on the heat transfer rate from a circular tube by using wind tunnel: An experimental view. *Heat Mass Transf.* **2018**, *54*, 3047–3057. [[CrossRef](#)]
10. Rai, A.; Bhuvad, S.S.; Sarviya, R.M. Enhancement of Heat Transfer in Perforated Circular Finned-Tube Heat Exchangers: A Numerical Investigation. *J. Phys. Conf. Ser.* **2020**, *1473*, 012024. [[CrossRef](#)]
11. Bisen, V.; Sagar, N.K. CFD Analysis of Heat Transfer in Annular Fins of various Profiles having different Shapes of Perforation. *Int. J. Res. Appl. Sci. Eng. Technol.* **2020**, *8*, 511–515. [[CrossRef](#)]
12. Bošnjaković, M.; Muhić, S. Numerical Analysis of Tube Heat Exchanger with Perforated Star-Shaped Fins. *Fluids* **2020**, *5*, 242. [[CrossRef](#)]
13. Chingulpitak, S.; Ahn, H.S.; Asirvatham, L.G.; Wongwises, S. Fluid flow and heat transfer characteristics of heat sinks with laterally perforated plate fins. *Int. J. Heat Mass Transf.* **2019**, *138*, 293–303. [[CrossRef](#)]
14. Gupta, M.; Yadav, S.; Kumar, R. Assessment of Effect of Perforated Fins on the Performance of Single Cylinder Engine. *Int. J. Res. Appl. Sci. Eng. Technol.* **2018**, *6*, 3051–3056. [[CrossRef](#)]
15. Lee, H.J.; Ryu, J.; Lee, S.H. Influence of perforated fin on flow characteristics and thermal performance in spiral finned-tube heat exchanger. *Energies* **2019**, *12*, 556. [[CrossRef](#)]
16. Karami, R.; Kamkari, B. Experimental investigation of the effect of perforated fins on thermal performance enhancement of vertical shell and tube latent heat energy storage systems. *Energy Convers. Manag.* **2020**, *210*, 112679. [[CrossRef](#)]
17. Bošnjaković, M.; Čikić, A.; Muhić, S.; Stojkov, M. Development of a new type of finned heat exchanger. *Tech. Gaz.* **2017**, *24*, 1785–1796. [[CrossRef](#)]
18. Bošnjaković, M.; Muhić, S.; Čikić, A.; Živić, M. How Big Is an Error in the Analytical Calculation of Annular Fin Efficiency? *Energies* **2019**, *12*, 1787. [[CrossRef](#)]
19. Bošnjaković, M.; Muhić, S.; Čikić, A. Experimental testing of the heat exchanger with star-shaped fins. *Int. J. Heat Mass Transf.* **2020**, *149*, 119190. [[CrossRef](#)]
20. Bošnjaković, M.; Čikić, A.; Muhić, S.; Holik, M. Heat Transfer, Correlations for Star-Shaped Fins. *Appl. Sci.* **2021**, *11*, 5912. [[CrossRef](#)]
21. Chabani, I.; Mebarek Oudina, F.; Ismail, A.I. MHD Flow of a Hybrid Nano-fluid in a Triangular Enclosure with Zigzags and an Elliptic Obstacle. *Micromachines* **2022**, *13*, 224. [[CrossRef](#)] [[PubMed](#)]
22. Djebali, R.; Mebarek-Oudina, F.; Choudhari, R. Similarity solution analysis of dynamic and thermal boundary layers: Further formulation along a vertical flat plate. *Phys. Scr.* **2021**, *96*, 085206. [[CrossRef](#)]
23. Rajeshkumar, M.; Logesh, K.; Thangaraj, M.; Govindan, S. Heat transfer study on finned tube heat exchanger using CFD. *Int. J. Ambient. Energy* **2021**, *42*, 239–243. [[CrossRef](#)]
24. Alkasassbeh, M.; Omar, Z.; Mebarek-Oudina, F.; Raza, J.; Chamkha, A. Heat Transfer Study of Convective Fin with Temperature-Dependent Internal Heat Generation by Hybrid Block Method. *Heat Transf. Asian Res.* **2019**, *48*, 1225–1244. [[CrossRef](#)]